SAND76-8039
Unlimited Release

Potential of a Solar Collector With a Stationary Spherical Reflector and a Tracking Absorber for Electrical Power Production

A. M. Clausing

Prepared by Sandia Laboratories, Albuquerque New Mexico 87115 and Livermore, California 94550 for the United States Energy Research and Development Administration under Contract AT (29-1)-789

Printed August 1976

When printing a copy of any digitized SAND Report, you are required to update the markings to current standards.

Sandia Laboratories
energy report

2900 QQB(3-74)

Issued by Sandia Laboratories, operated for the United States Energy Research and Development Administration by Sandia Corporation.

NOTICE

This report was prepared as an account of work sponsored by the United States Government. Neither the United States nor the United States Energy Research and Development Administration, nor any of their employees, nor any of their contractors, subcontractors, or their employees, makes any warranty, express or implied, or assumes any legal liability or responsibility for the accuracy, completeness or usefulness of any information, apparatus, product or process disclosed, or represents that its use would not infringe privately owned rights.

SAND76-8039
Unlimited Release
Printed August 1976

POTENTIAL OF A SOLAR COLLECTOR WITH A STATIONARY SPHERICAL REFLECTOR AND A TRACKING ABSORBER FOR ELECTRICAL POWER PRODUCTION

A. M. Clausing
Faculty Sabbatical Professor*
Solar Energy Technology Division 8184
Sandia Laboratories, Livermore

ABSTRACT

A fixed segment of a concave spherical mirror can be used to concentrate beam radiation onto a tracking absorber which pivots about the center of curvature of the mirror. A possible economic advantage of this system over concentrating collectors with tracking mirrors is reduced mirror cost. The characteristics of this system are analytically studied. The strong influences of the geometrical parameters of the stationary reflector/tracking absorber system are established. The penalty caused by the fixed reflector and the influence of the absorber temperature is also determined. The daily and yearly variations in the power produced by the system are presented.

*Associate Professor of Mechanical Engineering, University of Illinois at Urbana-Champaign, Urbana, IL.

CONTENTS

	Page
NOMENCLATURE	11
Introduction	13
Optical Characteristics of Collector	16
Model of SRTA Collector System	30
Results	34
Conclusions	45
APPENDIX--TABULATED DIURNAL VARIATIONS	47
References	51/52

ILLUSTRATIONS

Figure		Page
1.	Ray Pattern for Spherical Mirror With Rays Perpendicular to Plane of Aperture	13
2.	Reflecting Characteristics of Spherical Mirror With Rays at Angle of Incidence θ	14
3.	Cosine of Angle of Incidence Versus Time of Day, $(\ell - S) = 35°$	21
4.	Cosine of Angle of Incidence Versus Time of Day With Aperture Slope Equal to Latitude	23
5.	Average Daily Cosine (8 a.m. to 4 p.m.) Versus Time of Year	24
6.	The Influence of Day Length and Aperture Slope on the Average Yearly Cosine	26
7.	Diurnal Variations in Direct Normal Insolation and Collector Output at Vernal Equinox	37
8.	The Influence of Radiative and Convective Heat Losses	38
9.	Influence of Rim Angle on System Efficiency	39
10.	Influence of Concentration Ratio on System Efficiency	40
11.	Influence of Optical Losses on System Efficiency	42
12.	Influence of Time of Year and Aperture Slope on System Efficiency	43
13.	Comparison of Cosine, Optical, Thermal, and Carnot Losses	44

TABLES

Table		Page
I.	Influence of Rim Angle on Nominal Concentration Ratio	18
II.	Influence of Angle of Incidence and Rim Angle on the Effective Concentration Ratio	19
III.	Influence of Length of Day and $(\ell - S)$ on the Average Yearly Cosine	27
IV.	Flux Distribution on Cylindrical Receiver With $\phi = 60°$ and $\theta = 0°$	29
V.	Comparison of Predicted and Measured Direct Normal Insolations	31

NOMENCLATURE

A	area, m^2
C_1	constant used in Eq. (22)
CN	clearness number
CR	concentration ratio
d	declination, degrees
day	day of year
E	total energy, W-hr
h	hour angle, radians; convective heat transfer coefficient, W/m^2-K
I_{dn}	direct normal insolation, W/m^2
ℓ	latitude, degrees
n	number of reflections
p	power, W
q	heat flux, W/m^2
Q	heat flow rate, W
r	radial coordinate
S	slope, degrees
t	time, hours
T	temperature, K
y	coordinate
α	absorptance
γ	intercept factor
δ	blocking factor
ϵ	emittance

η	efficiency
θ	angle of incidence, degrees
ρ	reflectance
σ	Stefan Boltzmann's constant
τ	transmittance
ϕ	rim angle, degrees
ψ	sun's zenith, degrees

Subscripts

a	aperture or ambient
c	Carnot
e	effective
f	final value
H	hemispherical
L	loss
m	mirror
n	normal
o	optical
r	receiver
s	spherical or surroundings
ss	sunrise or sunset

POTENTIAL OF A SOLAR COLLECTOR WITH A STATIONARY SPHERICAL REFLECTOR AND A TRACKING ABSORBER FOR ELECTRICAL POWER PRODUCTION

Introduction

The stationary reflector/tracking absorber (SRTA) solar collector consists of a fixed segment of a concave spherical mirror that concentrates the sun's beam radiation onto a tracking absorber (Figure 1). The objective of this investigation is to determine the potential of this solar collector as an energy supply system for electrical power generation. Most of the analysis and many of the results which are presented, however, are of general value; therefore, they also could be used to determine the suitability of this collector system for other applications.

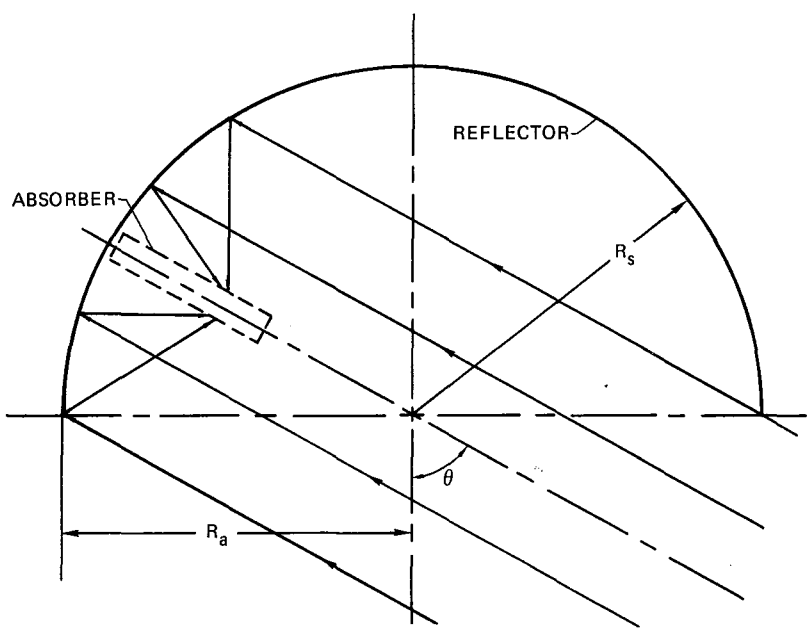

Figure 1. Ray Pattern for Spherical Mirror With Rays Perpendicular to Plane of Aperture

If the radius of the aperture of a spherical mirror R_a is much less than the radius of curvature R_s, parallel light perpendicular to the plane of the aperture would be focused essentially at a point. The point of focus would lie midway between the mirror and its center of curvature. In the proposed concentrator, R_a is of the same magnitude as R_s; hence, the focus becomes blurred due to spherical aberration. Figure 2 shows the ray pattern for a hemispherical mirror when the incident rays are parallel to the axis of the hemisphere. The parallel rays in this case are focused along a line which extends from the surface of the mirror to a distance of $R_s/2$ from this surface. Hence, an absorber which is to intercept all of the specularly reflected energy from such a spherical mirror must have a length of approximately $R_s/2$. Furthermore, since the spherical mirror is fixed, the absorber must be pivoted about the center of curvature of the mirror and track the sun in order to be kept at the line focus, parallel to the incident rays.

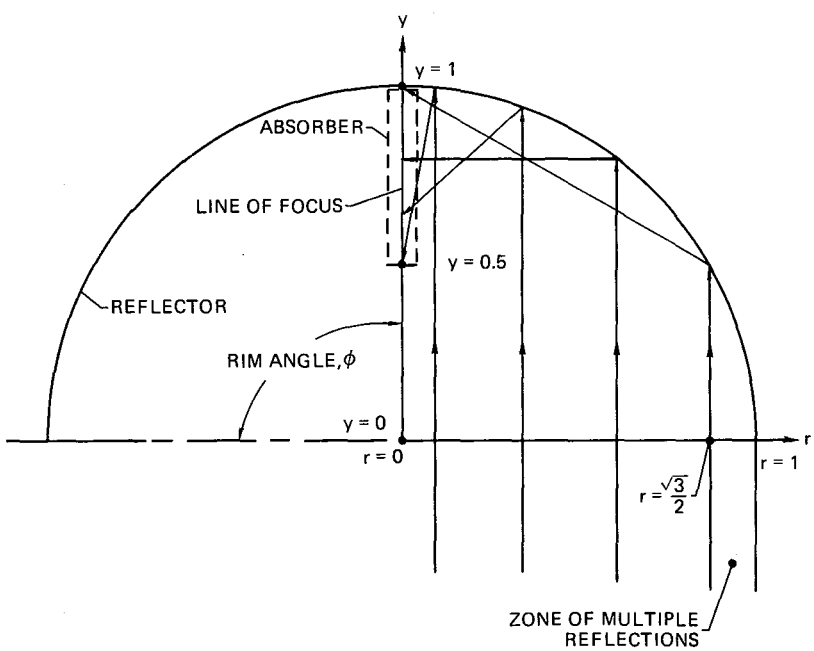

Figure 2. Reflecting Characteristics of Spherical Mirror With Rays at Angle of Incidence θ

The main advantage of the SRTA solar collector system is the fixed mirror. A fixed mirror enables the construction of extremely large units without prohibitive costs. For example, a spherical radiotelescope with a surface area of 7.49×10^4 m^2 (18.5 acres) was constructed near Arecibo, Puerto Rico. A large collector area reduces drastically the losses which occur in transporting the thermal energy to the heat engine, or the number of converters which are required if one is used in conjunction with each

collector. The cost of the plumbing should also be relatively low. In contrast, proposed arrays of paraboloids or parabolic cylindrical, solar collectors usually consist of such small collectors that transport losses, as well as the cost of the associated plumbing, can be appreciable. The central receiver is a notable exception; the energy is optically transmitted in this case from the relatively small heliostats to the receiver.

A major disadvantage of the SRTA collector system is the cosine loss. This loss is common to all collectors that do not track the sun. The direct solar radiation incident on a collector with a fixed aperture is proportional to the cosine of the angle of incidence θ, the angle between the sun's rays and the normal to the plane of the aperture. The angle of incidence is dependent on the time of the day, the time of the year, the latitude, and the orientation of the reflector. Severe degradation in performance occurs during portions of the year and at times during the day which are appreciably removed from solar noon. Since the convective and radiative losses from the absorber are relatively constant, the thermal efficiency of the collector system decreases with increasing θ at a rate considerably faster than the rate of decrease of the $\cos \theta$. Hence, the output of a fixed collector is generally a strong function of the time of the day with a sharp peak at solar noon. In contrast, fully tracking collectors have no cosine losses and single axis tracking parabolic cylindrical collectors with polar or north-south mounts have relatively small cosine losses. The central receiver system, on the other hand, has an appreciable cosine loss even with fully tracking heliostats. This is a consequence of an additional constraint--the redirection of the energy to the central receiver. However, the output of the central receiver system is relatively flat because portions of the field that perform best in the mornings or winter are partially balanced by other portions which perform best in the afternoons or summer.

The SRTA collector system was first described by Steward[1] who gave a brief qualitative description of the system. Steward and Kreith[2] recently published a more complete description, including an analysis of the axial variation of the concentration ratio; however, they did not consider the overall performance characteristics of the system. Kreider[3] analyzed the thermal performance of the SRTA collector, but his study did not include the diurnal or yearly variations.

The study described in this report is designed to establish the optical and thermal performance characteristics of the SRTA collector. Special emphasis is given to identifying the penalty associated with the fixed reflector. Construction problems, design details, and cost estimate are not considered. The daily output and system efficiency are based on clear days and an ideal thermal engine, a Carnot engine.

Optical Characteristics of Collector

Concentration Ratio

A fundamental parameter of any concentrating solar collector is the ratio of the heat flux on the receiver to the heat flux normal to the rays of the sun.* This ratio for the SRTA collector, in contrast to many concentrating collectors, is strongly dependent on the time of the day, the time of the year, the orientation of the fixed reflector, and the rim angle of the reflector. Like most other concentrating collectors, the flux concentration is further influenced by the accuracy of the mirror, the spectral reflectance of the mirror, the tracking accuracy, and component distortions caused by thermal and mechanical loads.

It is convenient in describing the effectiveness of SRTA concentrators to introduce a nominal concentration ratio. It is defined as the ratio of the aperture area to the receiver area**

$$CR \equiv \frac{A_a}{A_r} \tag{1}$$

Also, the nominal hemispherical concentration ratio is, by definition

$$CR_H \equiv \frac{\pi R_s^2}{A_r} \tag{2}$$

The usefulness of CR_H is not restricted to hemispheres. However, if the rim angle ϕ is 90°, $CR_H = CR$; hence the name nominal hemispherical concentration ratio. The minimum area of the receiver which is required to intercept the complete image of the sun is desired in order to obtain an upper bound for the concentration ratio.

Consider the image of the sun with perfect optics when the rays are perpendicular to the plane of the aperture as shown in Figure 2. The coordinates, which are normalized with respect to the radius of curvature R_s,

---

*The diffuse energy collected by the SRTA collector is generally negligible; therefore, it is ignored in all definitions and analyses.

**An external, non-cavity receiver geometry is assumed. The areas of the ends of the receiver are assumed to be perfectly insulated and are not included in the definition of A_r.

are also shown in this figure. It can easily be shown that the ray passing through the aperture at location r intercepts the y-axis at

$$y = \frac{1}{2(1-r^2)^{1/2}} \quad , \quad r \leq \sqrt{3}/2 \tag{3}$$

The rays passing through the aperture near r = 0 intercept the axis near y = 0.5; the ray passing through $r = \sqrt{3}/2$ intercepts the axis at y = 1; and all rays with $r > \sqrt{3}/2$ experience multiple reflections. The number of reflections n experienced by a ray before it passes through the axis of the mirror is

$$n = \left[\frac{\theta}{\pi - 2\theta}\right]^{*} + 1$$

where θ is the angle of incidence of the ray on the reflector. It can be shown from the geometry depicted in Figure 2 that

$$\theta = \sin^{-1} r$$

An equation for the point of intersection of the ray with the y-axis which is valid for any number of reflections is

$$y = \frac{r}{(-1)^{n-1} \sin(2n\theta)} \tag{4}$$

and the distance D the ray travels before intercepting the y-axis after n reflections can be shown to be

$$D = (n-1)\frac{\sin(\pi - 2\theta)}{\sin\theta} + \frac{\sin[(2n-1)\theta]}{\sin(2n\theta)} \tag{5}$$

Since the local radius of the receiver is much less than the radius of curvature of the mirror, Eq. (5) provides a good approximation for the distance the ray travels after its first reflection before it intercepts the absorber. The absorber diameter which is required to intercept the entire image of the sun with perfect optics and perfect tracking is dependent on this distance and the angle substended by the sun. The angle substended by the sun at mean sun-earth distance is 0.0093 radians.

---

*[x] denotes the greatest integer not greater than x.

Consider first the case of a rim angle of 60°; therefore, no multiple reflections occur with the collector-sun orientation shown in Figure 2. The required absorber diameter for this case at mean earth-sun distance varies linearly from 0.0046 R_S at y = 0.5 to 0.0093 R_S at y = 1; hence, the theoretical maximum nominal hemispherical concentration ratio is 288.

A 90° rim angle requires a wider absorber in the region y > 0.92, in order to account for the larger path lengths traveled by the multiply reflected rays. The required absorber diameter varies from 0.0046 R_S at y = 0.5 to 0.0146 R_S at y = 1. The variation is linear only from y = 0.5 to y = 0.92. The required increase in receiver area results in a theoretical maximum nominal hemispherical concentration ratio of 270.

The effects of multiple reflections are generally not negligible. For example, 25 percent of the rays undergo multiple reflections for the case depicted in Figure 2. A rim angle of 60° would result in no multiple reflections at normal incidence; however, multiple reflections still occur at all other angles of incidence. More generally, if the rim angle is greater than 45° and if the collector is to be utilized when the angle of incidence is greater than 45°, the minimum value of A_r is independent of rim angle and is a function only of the radius of curvature of the mirror. The theoretical maximum nominal hemispherical concentration ratio is a constant 270. Since the mirror accuracy and tracking accuracy should also be relatively independent of rim angle, it follows that

$$CR \cong CR_H \sin^2 \phi \tag{6}$$

Numerical values showing the influence of the rim angle on the nominal concentration ratio are given in Table I. These data show that the degree of concentration is drastically reduced with rim angles less than approximately 60°.

TABLE I

INFLUENCE OF RIM ANGLE ON NOMINAL CONCENTRATION RATIO

ϕ	90°	80°	70°	60°	50°	40°
CR/CR_H	1	0.97	0.88	0.75	0.59	0.41

The influence of the rim angle on the overall system efficiency will be shown later. The advantages of using rim angles less than 90° are a greater mirror utilization and a reduction in construction costs due to less mirror

area, less structural material, and simpler construction. The ratio of the mirror area to the aperture area is

$$\frac{A_m}{A_a} = \frac{2(1 - \cos\phi)}{\sin^2\phi} \tag{7}$$

Hence, the mirror area of a hemispherical reflector is twice the aperture area; whereas, it approaches the aperture area as the rim angle approaches zero.

The aperture of a fully tracking, concentrating paraboloid is always normal to the rays of the sun. The effective concentration ratio, which is defined as the ratio of the area of the aperture projected in a plane normal to the rays of the sun to the area of the receiver, is equal to the nominal concentration ratio for this or similar two-axis tracking reflectors. The effective concentration ratio CR_e for the fixed reflector of the SRTA system is

$$CR_e = CR \cos\theta$$

or

$$CR_e = CR_H \sin^2\phi \cos\theta \tag{8}$$

The influence of the angle of incidence θ for two rim angles, 90° and 60°, is given in Table II. It is seen that for angles of incidence greater than 60° the incident energy flux is reduced to less than half of that which is incident on a tracking reflector. For example, the angle of incidence at solar noon on winter solstice for a horizontal aperture at a north latitude of 33.65° is 57°. Hence, the effective concentration ratios, for rim angles of 90° and 60° and a nominal hemispherical concentration ratio of 100, are only 54 and 40, respectively, even at solar noon. This disadvantage of the SRTA system, especially at non-ideal times of the year, is self-evident.

TABLE II

INFLUENCE OF ANGLE OF INCIDENCE AND RIM ANGLE ON THE EFFECTIVE CONCENTRATION RATIO (CR_e/CR_H)

ϕ \ θ	0°	15°	30°	45°	60°	75°
90°	1	0.97	0.87	0.71	0.50	0.26
60°	0.75	0.72	0.65	0.53	0.37	0.19

Cosine Loss

Equation (8) and Table II show the influence of the angle of incidence on the effective concentration ratio. The diurnal and yearly variation of this angle and the influence of aperture slope remain to be described. Simultaneously, a more important question can be addressed--the determination of the cosine loss. Since the solar intensity is nearly flat over a sizable portion of the day,* the cosine of the angle of incidence averaged over the day (the average daily cosine) and averaged over the year (the average yearly cosine) give indications of the fraction of energy lost with a fixed reflector or with a single axis of tracking. Since the heat losses from the receiver are relatively constant, the overall reduction in system performance is greater than that indicated by the deviation of the average cosine from unity.

A nonperformance aspect of choosing the slope of the aperture and the size of the collector is the visual impact. The height of the upper lip, or more precisely, the difference between the elevation of the highest and lowest point on the rim of the reflector H is

$$H = 2 \sin S \sqrt{\frac{A_a}{\pi}} \tag{9}$$

It will be assumed that the aperture azimuth angle (the angle measured in the horizontal plane from south to the horizontal projection of the normal to the aperture) is zero. The tilt or slope of the collector S is defined as the angle between the rear face of the plane of the aperture and the horizontal plane. The optimum slope is to be determined. It is not difficult to show that the cosine of the angle of incidence is:

$$\cos \theta = \sin d \sin (\ell - S) + \cos d \cos h \cos (\ell - S), \quad |h| < h_{ss} \tag{10}$$

where d is the sun's declination, ℓ is the latitude, h is the hour angle, and h_{ss} is the hour angle at sunset. Equation (10) shows that the angle of incidence is a function only of the declination, the hour angle, and the difference between the latitude and slope (ℓ-S).

The diurnal variations of the cosine of θ at summer solstice, equinox, and winter solstice are given in Figure 3 for (ℓ-S) equal to 35°; for example, a horizontal aperture at a north latitude of 35°. The poor performance during

*Experimental data are given in Table V and Figure 7 which show typical diurnal variations of the beam or direct insolation.

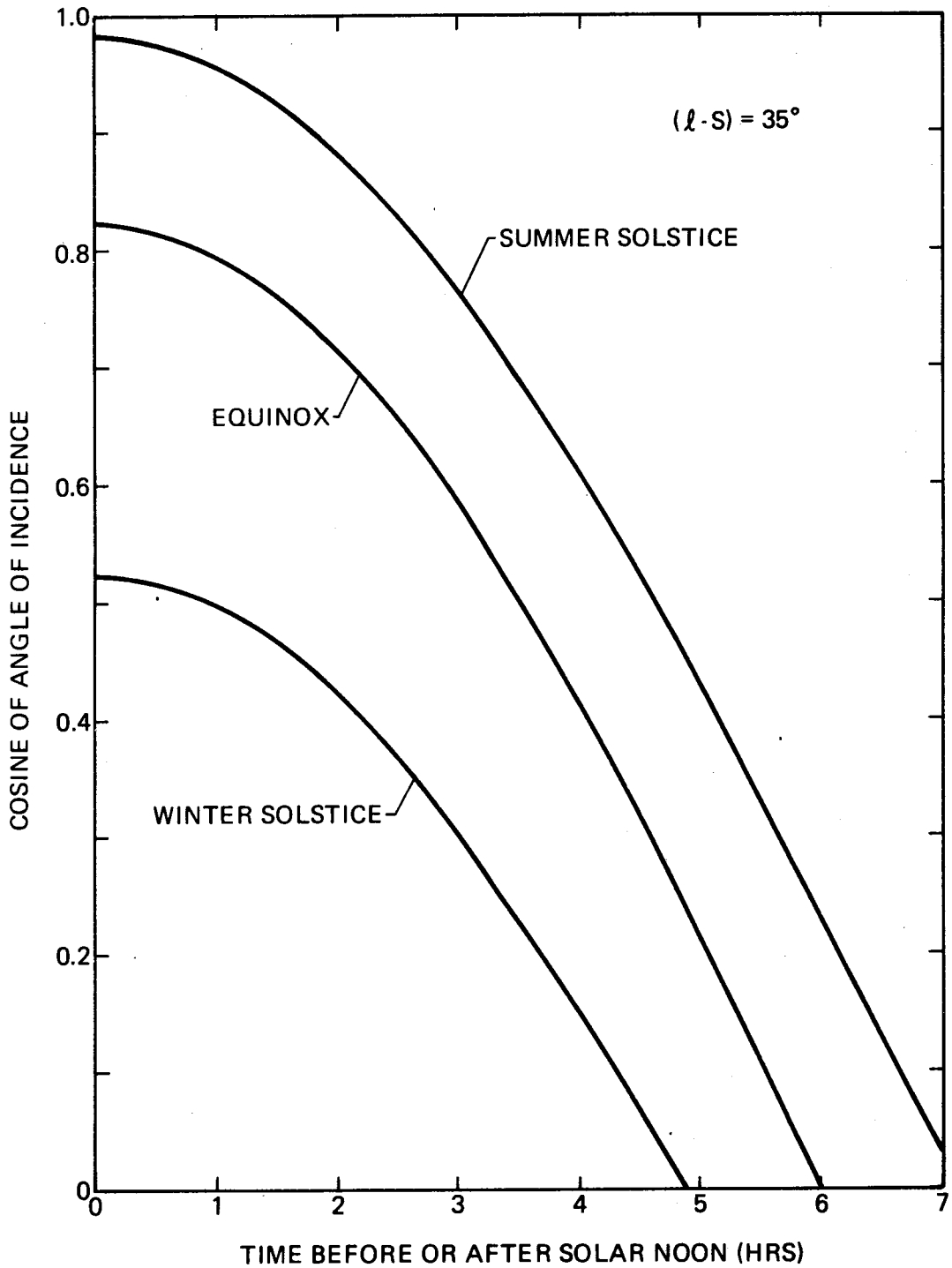

Figure 3. Cosine of Angle of Incidence Versus Time of Day, $(\ell - S) = 35°$

the winter with this collector orientation is probably unacceptable. If S is equal to ℓ, Eq. (10) reduces to

$$\cos\theta = \cos d \cos h, \qquad S = \ell \tag{11}$$

Figure 4 gives the diurnal variations with $S = \ell$ at equinox, summer solstice, and winter solstice. These results and Eq. (11) both show that if atmospheric attenuation is neglected, a collector with $\ell = S$ performs as well during sunlit hours at winter solstice as it does at summer solstice. This performance is considerably better than the equinox performance with $\ell - S = 35°$ shown in Figure 3. Since the early and late portions of the day are of little importance due to the overall low efficiency at such times, the equinox performance of the tilted collector given in Figure 4 is about the same as the summer solstice performance of the collector with $\ell - S = 35°$ (see Figure 3). Thus the performance during two-thirds of the year has been vastly improved, and the performance during the remaining third of the year, centered around summer solstice, has not changed significantly.

The average daily cosine is desired in order to obtain an indicator of the fraction of the available energy which is intercepted by a collector with a fixed mirror. A collection period centered about solar noon of length $2\,t_f$ is of interest. The average daily cosine is

$$\overline{\cos\theta}\,\Big|_{day} = \frac{1}{t_f}\int_0^{t_f} \cos\theta \, dt \tag{12}$$

where the time t is measured from solar noon. If Eq. (10) is substituted into Eq. (12) and the small variation in the sun's declination throughout the day is neglected, one obtains

$$\overline{\cos\theta}\,\Big|_{day} = \sin d \sin(\ell - S) + \cos d \cos(\ell - S)\,\frac{\sin h_f}{h_f}, \quad h_f > h_{ss} \tag{13}$$

Equation (13) is only meaningful if $h_f > h_{ss}$. The variation of the average daily cosine throughout the year is shown in Figure 5. Values of $(\ell - S)$ between 0 and 50 degrees are considered, and an eight hour day is assumed. The poor performance from autumnal equinox through vernal equinox for collectors with $(\ell - S)$ greater than approximately 20° is clearly shown in Figure 5. If $(\ell - S)$ is zero, the variation in the average daily cosine throughout the year is only ± 4.3 percent of its mean value.

If the average daily cosine is integrated over the year, an indication of the influence of day length and collector slope on the total yearly output of the collector is obtained. The yearly average cosine is defined as:

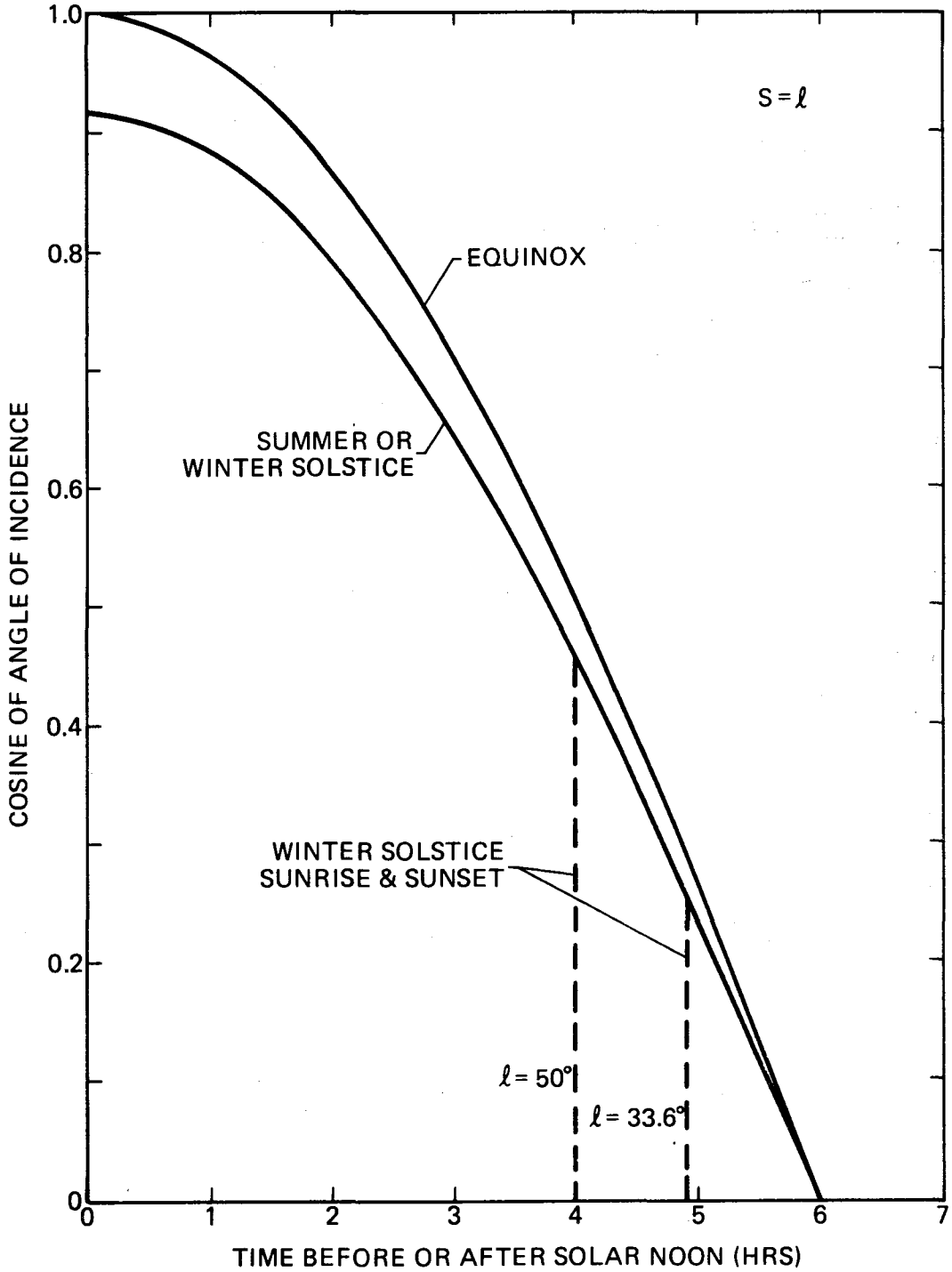

Figure 4. Cosine of Angle of Incidence Versus Time of Day With Aperture Slope Equal to Latitude

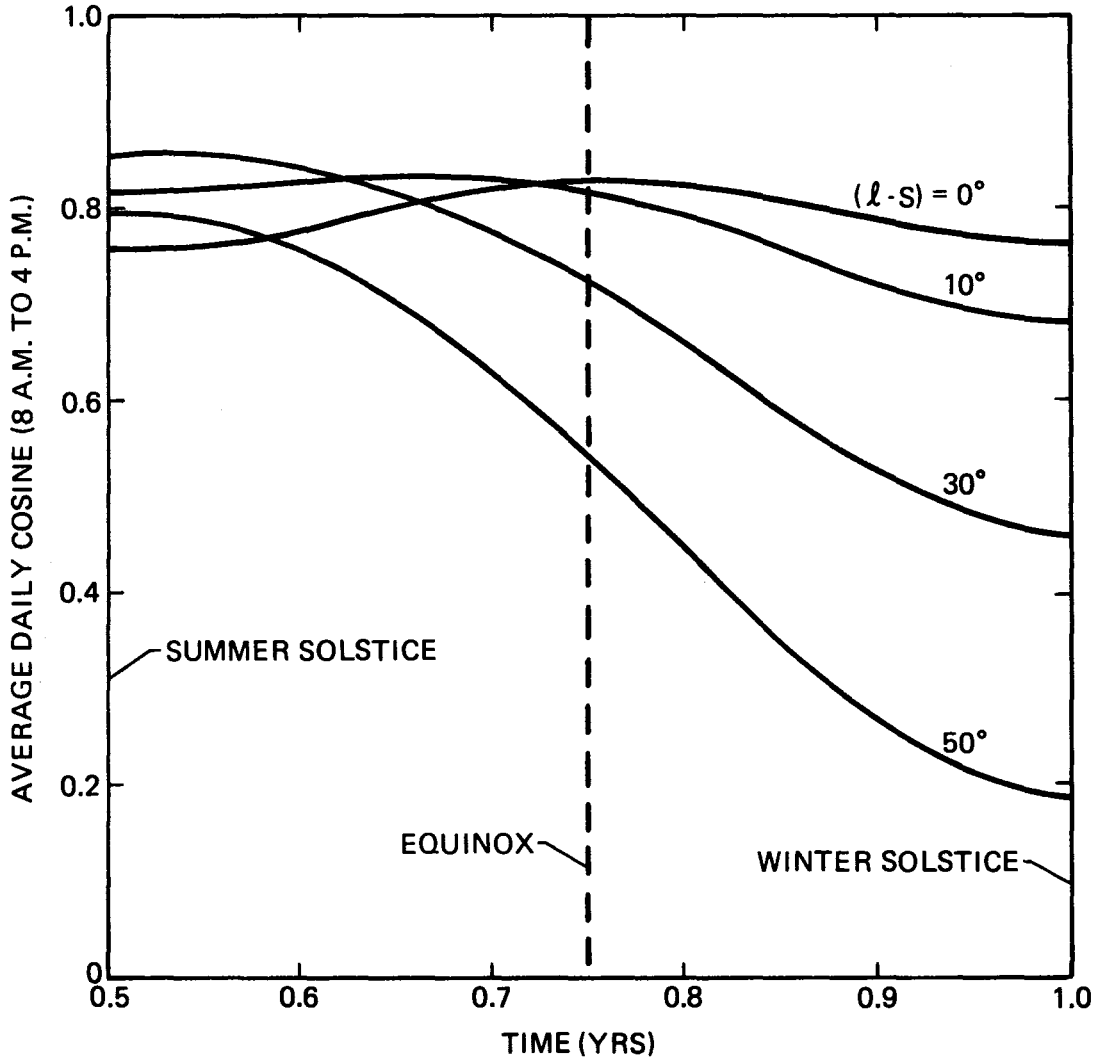

Figure 5. Average Daily Cosine (8 a.m. to 4 p.m.) Versus Time of Year

$$\overline{\cos\theta}\,\Big|_{yr} = (yr)^{-1}\int_0^{1\ yr} \overline{\cos\theta}\,\Big|_{day}\, dt \tag{14}$$

where t is the time in years. If Eq. (13) is substituted into Eq. (14), one obtains

$$\overline{\cos\theta}\,\Big|_{yr} = A_1 \sin(\ell\text{-}S) + A_2 \frac{\cos(\ell\text{-}S)\sin h_f}{h_f}\ , \quad h_f > h_{ss} \tag{15}$$

where

$$A_1 = (yr)^{-1}\int_0^{1\ yr} \sin d\ dt \tag{16}$$

and

$$A_2 = (yr)^{-1}\int_0^{1\ yr} \cos d\ dt \tag{17}$$

Equation (15) is meaningful only if h_f is greater than h_{ss} at winter solstice. If the sun's declination is obtained from the 1977 Ephemeris,[4] one obtains $A_1 = 0.0067$ and $A_2 = 0.9592$;* whereas, the ASHRAE approximation for the sun's declination[5] gives $A_1 = 0.0059$ and $A_2 = 0.9593$,* a negligible difference. The use of Eq. (15) greatly simplifies the evaluation of collector performance since it enables the calculation of average yearly cosines at any latitude for any collector slope and applicable day length without performing any numerical integrations.

The variation of the average yearly cosine with (ℓ-S) is shown in Figure 6 for day lengths ranging from four hours to twelve hours. Tabulated values are also provided in Table III. The restriction $h_f > h_{ss}$ means that the maximum latitudes at which these results can be applied are 63.4°, 58.5°, 49.1°, 30.8°, and 0° for day lengths of 4, 6, 8, 10, and 12 hours, respectively.

Since A_1 is small, the value of (ℓ-S) which results in the maximum average yearly cosine is approximately zero for all day lengths. The curves given in Figure 6 show that the average daily cosine is only a weak function of (ℓ-S) if (ℓ-S) is small. Specifically, (ℓ-S) of 10° results in approximately a 1.4 percent reduction in the average yearly cosine and (ℓ-S) of 20° results in approximately a 5.7 percent reduction. The magnitude of these reductions

---

*Estimates of the error in the numerical integrations showed that all of the numerical results are accurate to the four decimal places which are provided.

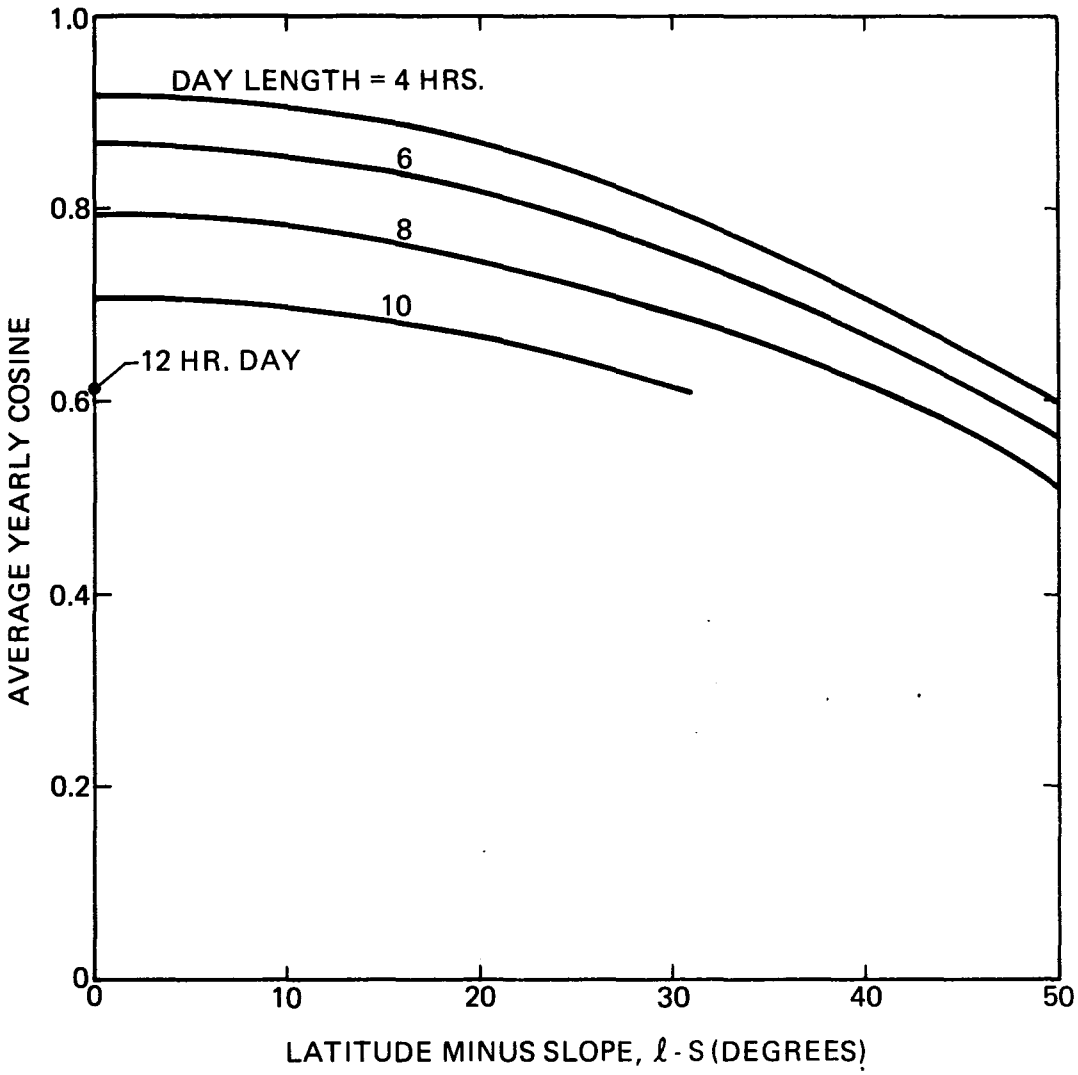

Figure 6. The Influence of Day Length and Aperture Slope on the Average Yearly Cosine

TABLE III

INFLUENCE OF LENGTH OF DAY AND (ℓ-S) ON THE AVERAGE YEARLY COSINE

	Length of Day (hrs)					
(ℓ-S)	2	4	6	8	10	12
0	0.948	0.916	0.864	0.793	0.708	0.611
5	0.945	0.913	0.861	0.791	0.706	---
10	0.935	0.903	0.852	0.782	0.698	---
15	0.918	0.887	0.836	0.768	0.685	---
20	0.893	0.863	0.814	0.748	0.667	---
30	0.825	0.797	0.751	0.690	0.616	---
40	0.731	0.706	0.666	0.612	---	---
50	0.615	0.594	0.560	0.515	---	---

is only weakly dependent on the day length. Since A_1 is small, the average yearly cosine with (ℓ-S) = β is approximately equal to the average yearly cosine with (ℓ-S) = $-\beta$.

Although average cosines give a good indication of the penalty caused by the fixed reflector and the influence of the collector slope, these results must be interpreted carefully. They do not include the influence of atmospherical attenuation of the beam radiation, and require a uniform distribution of clear weather throughout the day and year. The average yearly cosines are based on a fixed length day; a more meaningful but less convenient criterion for the termination of the integration would be a minimum level of insolation on the collector aperture. Since the average daily cosine is a strong function of the time of the year only for large values of (ℓ-S), the two criteria will give similar results when (ℓ-S) is small.

Optical Losses

One source of optical loss is the failure of the concentrator to collect diffuse radiation. This loss is common to most concentrators and is being ignored. The remaining optical losses are: blocking losses, reflection losses, intercept losses, transmission losses, and absorption losses. The first attenuation experienced by the incident beam radiation is the blocking loss. The absorber, the tracking boom, the counterbalance, and the boom support struts all shade the reflector. (The self-shading of the reflector is excluded from the optical losses; it is implicit in the cosine loss.) Hence

only the fraction δ of the energy which is incident on an identical, bare reflector reaches the actual reflector. A realistic range of δ for the SRTA collector is probably

$$0.95 < \delta < 0.99 \tag{18a}$$

The reflection loss, the next attenuation experienced by the beam, is a consequence of having a mirror which is not a perfect specular reflector. The specular reflectance ρ is the fraction of the incident beam radiation which is specularly reflected. A realistic range for ρ is probably

$$0.7 < \rho < 0.9 \tag{18b}$$

It should be remembered in choosing a representative value for ρ that part of the beam radiation undergoes more than one reflection.

The third loss experienced by the beam is the intercept loss. Only the fraction γ of the specularly reflected energy is intercepted by the absorber due to imperfect optics and tracking, and blockage by system components. An absorber which is sufficiently large to account for the effects of imperfect tracking and imperfect optics would result in excessive heat loss. The optimum value of the intercept factor probably lies in the range

$$0.85 < \gamma < 0.98 \tag{18c}$$

Finally, not all of the energy which is incident on the aperture of the receiver is absorbed. If a cover plate is used over the absorber surface, only the fraction τ of the incident energy is transmitted through the cover plate. The transmittance of typical cover plate materials is strongly dependent on the angle of incidence as well as the spectrum of the incident energy. The large incidence angles of much of the energy incident on the tracking absorber of the SRTA collector probably means that transmission losses will be too high if cover sheets are used. The practical range of the transmittance is

$$0.7 < \tau \leq 1.0 \tag{18d}$$

where 1.0 corresponds to the absence of a cover plate. The absorptance α is the fraction of the incident energy which is absorbed. The spectrum of the incident energy, the angle of incidence, the temperature of the absorbing surface, and the geometry of the receiver all influence this ratio. Since a cavity type receiver appears unsuitable, a realistic range of the absorptance is

$$0.8 < \alpha < 0.95 \tag{18e}$$

The fraction of the incident energy which is absorbed by the absorbing surfaces of the receiver is $\delta\rho\gamma\tau\alpha$, which will be defined as the optical efficiency η_0. The overall system performance is dependent on the product of these five quantities and not their individual values. The range of η_0, based on the limits given in Equations (18a) through (18e), is

$$0.3 < \eta_0 < 0.8 \tag{19}$$

The influence of the optical losses on the overall system efficiency is established in the section entitled "Results."

Heat Flux Distribution

The relatively large receiver required in the SRTA collector system may be partially offset in some applications by the nonuniform energy distribution along the "line" focus. For example, if a constant diameter, circular cylinder is used as the absorber with a reflector having a 60° rim angle, the ratio of the local heat flux on the receiver q_r to the average $\overline{q}_r$ when the sun's rays are normal to the aperture is

$$\frac{q_r}{\overline{q}_r} = \frac{4}{3} r \frac{dr}{dy} = \frac{1}{3y^3} \quad , \quad 0.5 < y < 1 \tag{20}$$

The numerical values given in Table IV show that the flux at y = 0.5 is 8/3 times as large as the average flux. Unfortunately, this distribution is dependent on the angle of incidence of the sun's rays. Hence the flux distribution is dependent on both the time of the year and the time of the day, and a strong circumferential variation in the flux distribution arises whenever θ is large. Designing an optimum receiver for the SRTA collector system for these reasons is probably a more difficult task than for any other collector system.

TABLE IV

FLUX DISTRIBUTION ON CYLINDRICAL RECEIVER WITH ϕ = 60°, θ = 0°

y	0.5	0.6	0.7	0.8	0.9	1.0
$q_r/\overline{q}_r$	2.67	1.54	0.97	0.65	0.46	0.33

Model of SRTA Collector System

The following assumptions and conditions are employed in the evaluation of the SRTA collector.

(i) A clear day and the validity of a modified ASHRAE model for the calculation of direct insolation are assumed. A simple expression proposed by ASHRAE[5] for the direct normal insolation is:

$$I_{dn} = CN \cdot f_1(\text{day}) \cdot \exp\left[-f_2(\text{day})/\cos\psi\right] \tag{21}$$

where CN is the clearness number (see Reference 6), ψ is the sun's zenith angle, and f_1 and f_2 are prescribed functions of the day of the year. A comparison of Eq. (21) with data from Inyokern and Goldstone showed good agreement at solar noon, but the model predicted too much attenuation at large zenith angles. Hence Eq. (21) was modified empirically in order to obtain better agreement with experimental data. Several different expressions were tried; the one which gave good agreement to within approximately an hour of sunrise or sunset was:

$$I_{dn} = CN \cdot f_1(\text{day}) \cdot \exp\left[\frac{-f_2(\text{day}) \cdot (1 + C_1/\cos\psi_0)}{\cos\psi + C_1}\right] \tag{22}$$

where ψ_0 is the zenith angle at solar noon, and a value of 0.2 was used for the constant C_1. Equation (22) differs appreciably from Eq. (21) only at large zenith angles. A comparison between Eq. (22) and experimental data is given in Table V.

(ii) A clearness number of 1.0 was used throughout the year (see Reference 6). A north latitude of 33.65 degrees was assumed.

(iii) An isothermal absorber was used in the analysis. In practice, the receiver would probably not be isothermal; however, a more realistic description requires specification of heat transfer fluids used in the absorber, the parameters of the thermal cycle, etc. In addition, temperature drops occur: (a) between the surface of the receiver and the heat transfer fluid used in the absorber,

TABLE V

COMPARISON OF PREDICTED AND MEASURED DIRECT NORMAL INSOLATIONS

	Intensity of Direct Normal Radiation (W/m^2)							
	Day = 358 (≃ Winter Solstice) Inyokern, 1963		Day = 83 (≃ Vernal Equinox) Inyokern, 1963		Day = 173 (Summer Solstice) Inyokern, 1963		Day = 342 Goldstone, 1974	
Hours Before or After Sunset	Data	Model*	Data	Model*	Data	Model*	Data	Model*
0	910	903	930	991	910	942	935	907
1	905	894	925	986	920	937	928	898
2	860	863	915	968	935	924	895	868
3	780	798	890	935	930	898	815	805
4	675	665	835	873	895	854	615	680
5			765	752	825	782		
6					720	656		
Sunset:	4:50 PM		6:03 PM		7:13 PM		4:52 PM	

*$C_1 = 0.2$

(b) along the piping which transports the thermal energy from the receiver to the thermal engine or the heat exchanger if an intermediate loop is used, and (c) in intermediate heat exchangers if required. Considering these factors and other losses, the heat loss with an isothermal receiver is not expected to exceed the total loss from a nonisothermal receiver which delivers a working fluid to the thermal engine at the assumed receiver temperature T_r.

(iv) The efficiency of the thermal engine which is used to convert the thermal energy to electrical energy was assumed to be equal to the Carnot efficiency, which is

$$\eta_c = 1 - \frac{T_{sink}}{T_r} \tag{23}$$

Since no engine operating between two given temperatures can be more efficient than a Carnot engine operating between the same two temperatures, the use of this efficiency provides an upper bound for the electrical power that could be produced.

(v) The absorber was assumed to be semi-gray with a solar absorptance α and an infrared emittance ϵ. The surroundings were assumed to be black (by virtue of geometry) at a uniform temperature T_s. The analysis is valid for any receiver shape as long as the view factor of the receiver with itself is small. The absorptance was assumed to be independent of the angle of incidence. Recent measurements[7] show an appreciable decrease of the solar absorptance of Harshaw black chrome on bright nickel substrate at large angles of incidence. Since large angles of incidence are common with the SRTA collector system, this phenomenon could cause a significant reduction in the absorptance for some surface preparations.

(vi) The absence of a cover plate over the absorber surface was assumed in the calculation of the convective heat loss. Since the heat transfer coefficient due to natural convection in air is nearly independent of Δt for the conditions of this study (in fact, the Grashof number actually decreases slightly with increasing absorber temperature), the convective heat exchange between the absorber and the ambient air at temperature T_a was based on a constant heat transfer coefficient of 8 W/m^2-K (1.4 BTU/hr-ft^2-°F). A natural wind, or a wind created by the hot air flowing up out of the

reflector bowl, could account for slightly higher heat losses by convection. An ambient temperature T_a of 20°C was used.

(vii) The specular reflectance ρ of the mirror was assumed to be independent of wavelength and angle of incidence. It was further assumed that all rays undergo a single reflective loss. The maximum percent of the energy which can undergo two or more reflections is 25 percent. The effect of multiple reflections could be partially accounted for by an artificial reduction in the reflectance.

(viii) All heat losses other than convective and radiative losses from the receiver surface were neglected. Also the heat loss from the ends of the receiver was neglected.

(ix) The approximation for the sun's declination proposed by ASHRAE[5] is used.

The heat loss Q_L from the receiver with the simplifying assumptions which are stated is

$$Q_L = h A_r (T_r - T_a) + \sigma \epsilon A_r (T_r^4 - T_s^4) \tag{24}$$

where h is the average convective heat transfer coefficient, A_r is the area of the receiver, and σ is the Stefan-Boltzmann constant. The incident solar energy absorbed by the receiver is:

$$Q = A_a (\delta \rho \gamma \tau \alpha) I_{dn} \cos\theta$$

or

$$Q = A_r (CR) \eta_0 I_{dn} \cos\theta \tag{25}$$

where I_{dn} is the direct normal insolation, η_0 is the optical efficiency, and θ is the angle of incidence. The net thermal output of the collector is

$$Q_{net} = (Q - Q_L)$$

and the electrical power produce with an ideal Carnot engine is

$$P = \eta_c (Q - Q_L)$$

The energy produced from time t before solar noon to time t after solar noon is

$$E = 2 \int_0^t P\, dt$$

In addition to the power P and the energy E, two instantaneous efficiencies were calculated. One, η_a, was 100 percent times the power divided by the rate of incident energy on the fixed aperture, and the other, η_n, is identical to η_a except the aperture area is assumed to be normal to the sun's rays. The instantaneous power produced per unit area of mirror surface was also determined.

Probably the most meaningful efficiency is the overall system daily efficiency η which is defined as

$$\eta = 100 \frac{\int_0^{t_f} (Q - Q_L)\eta_c \, dt}{\int_0^{t_{ss}} I_{dn} A_a \, dt} \tag{26}$$

where t = 0 corresponds to solar noon, t_{ss} the time from solar noon to sunset, and t_f is the time at which $(Q - Q_L)$ becomes negative. The overall system daily efficiency is 100 times the daily energy output of the engine divided by the total energy incident on a tracking plane surface of area A_a. This efficiency is considered a meaningful barometer of the system performance and is used extensively in the parametric studies.

Results

Several variables within their typical range have a minor influence on the performance of the SRTA collector system. Hence these quantities are held constant in the parametric studies in order to reduce the number of variables and simplify the presentation of the results. Specifically, these quantities are the ambient temperature T_a, the temperature of the surroundings T_s, and the convective heat transfer coefficient h (see discussion in previous section). Most of the results are independent of the area of the aperture A_a, and the dimensional results which are not can be easily modified for different values of this parameter. The result also can be easily adjusted for different sink temperatures. Hence both A_a and T_{sink} were held constant.

Results previously given showed that: (1) the optimum slope for year-around, clear weather performance was equal to the latitude and (2) a slope 10 degrees greater than or less than the latitude caused a change in the average yearly cosine of less than 2 percent. Hence the collector was assumed to be tilted toward the south at an angle equal to the latitude. Once (ℓ-S) is fixed, the latitude plays a minor role. It has a secondary influence on the direct normal insolation and effects the length of the day. A constant north latitude of 33.65 degrees was used in all parametric studies. This latitude is probably within 5° of most sites proposed for solar electric power generation in the United States. A clearness number of one was used in the

model for the direct normal insolation. The longitude influences only the clearness number and the relationship between solar time and standard time. Since a clearness number of one was specified, the longitude does not influence the results to be presented.

Variables which have an appreciable influence on the performance of the SRTA collector are: receiver temperature, optical efficiency, time of year, rim angle, concentration ratio, and emittance of absorber. The influence of these variables will be parametrically shown. A set of representative parameters were chosen as the standard case in order to facilitate comparisons. Specifically:

ϵ (emittance) = 0.22--It appears that a cavity absorber is not practical in conjunction with the fixed mirror concept. Hence a selective surface is highly desirable in order to reduce radiation losses. An emittance of 0.22 appears to be an attainable goal with a solar absorptance of about 0.9, an α/ϵ of 4. It should be remembered that the absorber surface will be in air at a temperature of near 500°C.

CR_H (nominal hemispherical concentration ratio) = 100--It was shown that the theoretical maximum nominal hemispherical concentration ratio was 270. Considering realistic tracking errors, mirror errors, and an intercept factor near 0.95, a value of CR_H of 100 was chosen for the standard case.

η_0 (optical efficiency) = 0.76--The optical efficiency is the product of $\rho\ \alpha\ \tau\ \delta\ \gamma$. A spectral reflectance ρ of between 0.85 and 0.9 is typical for high quality mirrors. The solar absorptance of a selective surface characteristically lies between 0.85 and 0.95. The use of a cover plate seems illogical due to the high reflective loss for rays at large angles of incidence; hence $\tau = 1$. Values of δ and γ of 0.99 and 0.95 respectively are projected. These values give $0.68 \leq \eta_0 \leq 0.80$. A value of 0.76 at the high end of this range was chosen.

Day = 81--Since the overall system daily efficiency is within several percent of its value at equinox during two-thirds of the year, vernal equinox was chosen for the standard case.

ϕ (rim angle) = 90°--This rim angle results in the highest system efficiency; therefore, it provides a convenient upper bound.

T_r (receiver temperature) = 500°C--The influence of the receiver temperature is very strong; therefore, results are generally given for all values of T_r ranging from 200°C (392°F) to 550°C (1022°F). If a range of T_r is not provided, 500°C (932°F) is used. Summarizing, the standard case uses:

$A_a = 10^4\ m^2$; CR = 100; S = 34°; ϕ = 90°; $T_a = T_s$ = 20°C (68°F); h = 8 W/m^2-K (1.4 BTU/hr-ft^2-°F); T_{sink} = 40°C (104°F); ϵ = 0.22; η_0 = 0.76; Day = 91; CN = 1.0; C_1 = 0.2; ℓ = 33.65°, and T_r = 500°C (932°F).

If any variable differs from this standard set, its value will be specified.

Three sets of tabulated results are given in the Appendix which show the diurnal variation at winter solstice, vernal equinox, and summer solstice of: the sun's altitude angle, the sun's azimuth, the angle of incidence, the direct normal insolation, the heat flux through the aperture, the net heat flux through the receiver, the instantaneous power, the total power generated from time t before solar noon to time t after solar noon, the system total daily efficiency, the instantaneous efficiencies, η_a and η_n, and the instantaneous power per unit mirror area.

A comparison between the diurnal variations in the collector instantaneous output and the direct normal insolation is given in Figure 7. The direct normal insolation and the collector output are both normalized with respect to their respective values at solar noon. The direct normal insolation predicted by the model as well as experimental data from a clear day near vernal equinox at Inyokern, California, are provided. The model and experimental data agree well and show high values of the direct normal insolation throughout the day with an attenuation of less than 25 percent at one hour before sunset or after sunrise. In contrast, the collector output is sharply peaked and is attenuated by more than 50 percent at 2-1/2 hours before sunset or after sunrise. This sharp peak is a consequence of the fixed reflector.

The influence of the emittance of the selective surface on the overall system daily efficiency is shown in Figure 8. The efficiency of the convertor, the Carnot efficiency, dominates the overall system efficiency at low temperatures. The influence of the emittance is readily discernible only at temperatures above approximately 250°C. The influence of α/ϵ rapidly decreases as α/ϵ nears ten; the main gain has already been realized at α/ϵ of four. The contribution of the convective loss can be established by comparing the case of no convective and radiative losses, the dashed curve in Figure 8, with the case of no radiative loss $\alpha/\epsilon = \infty$.

The influence of the rim angle on the overall system efficiency is shown in Figure 9. Rapid deterioration in performance begins to occur with decreasing rim angle at approximately 70°. This conclusion could also be inferred from Eq. (6) or Table I. The influence of the rim angle is also implicit in the results given in Figure 10 which shows the effect of the nominal concentration ratio on the overall system daily efficiency. The change

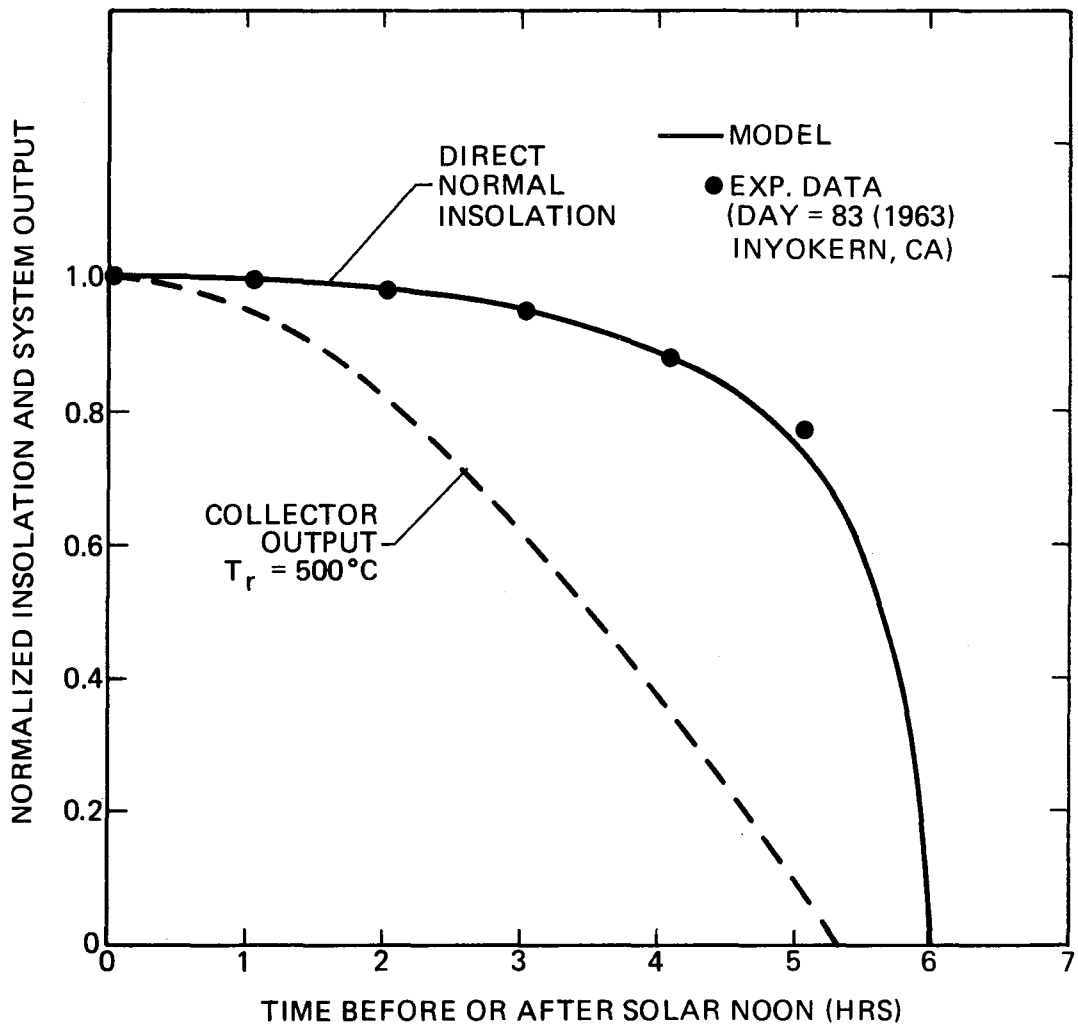

Figure 7. Diurnal Variations in Direct Normal Insolation and Collector Output at Vernal Equinox

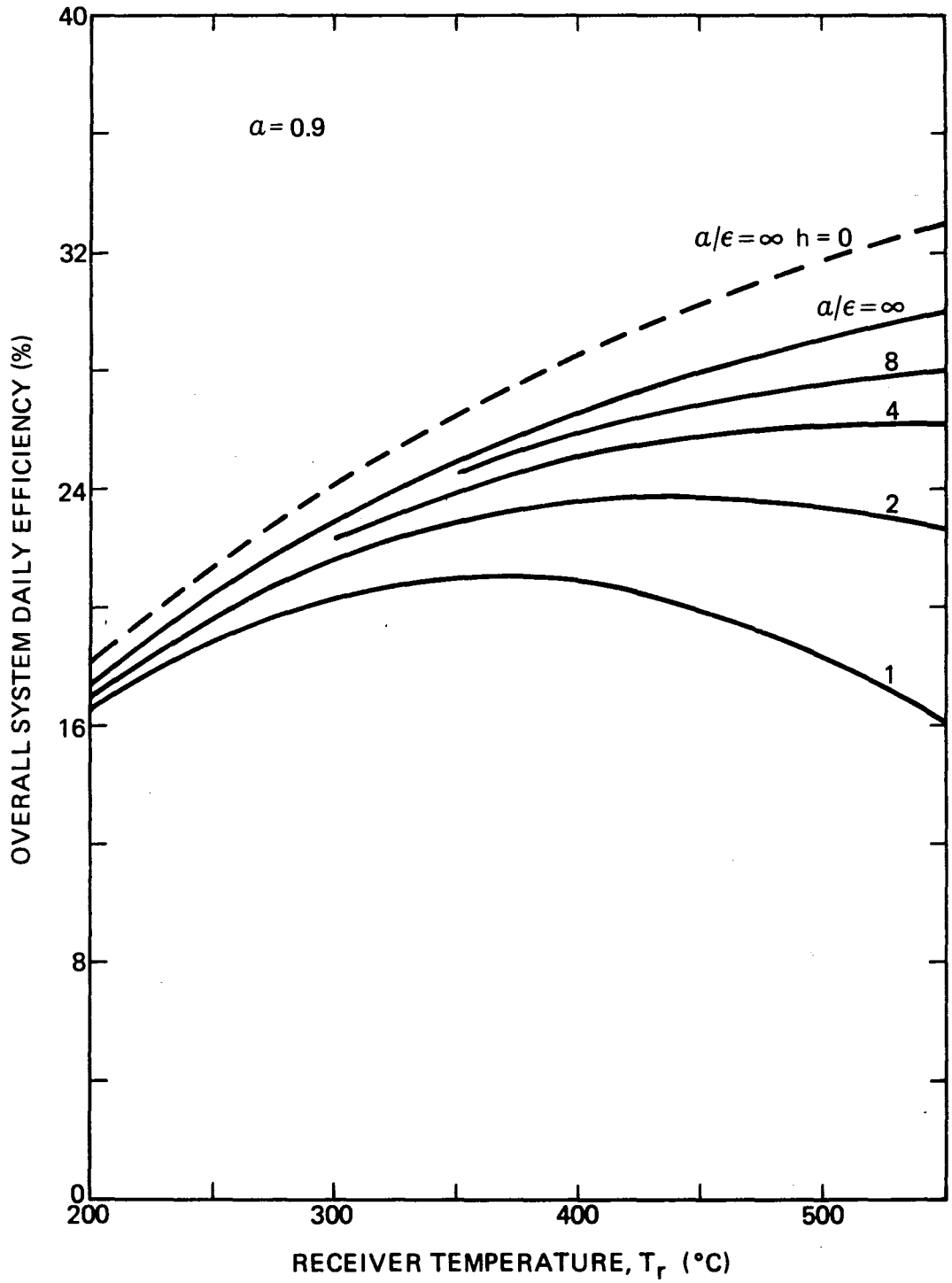

Figure 8. The Influence of Radiative and Convective Heat Losses

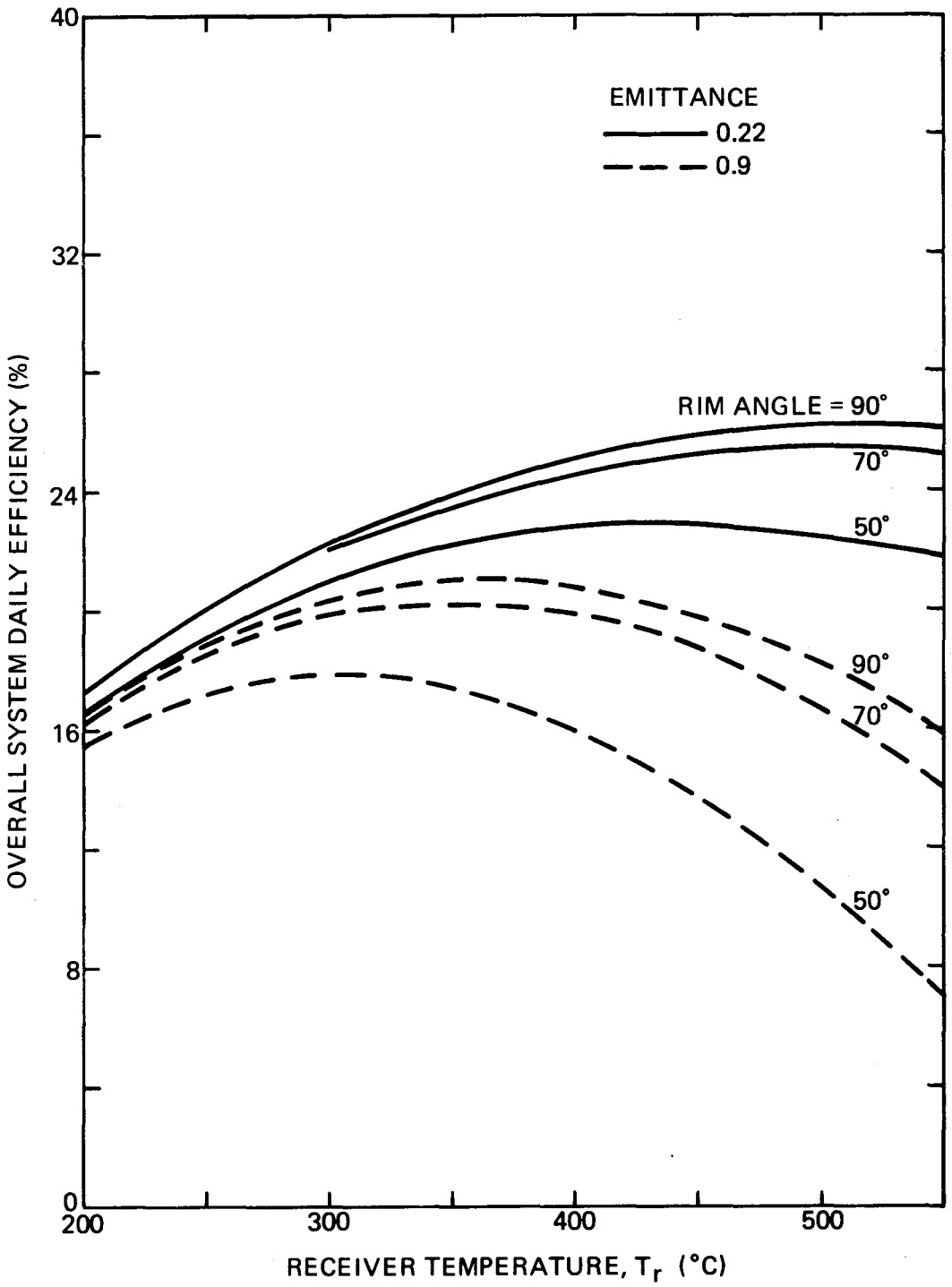

Figure 9. Influence of Rim Angle on System Efficiency

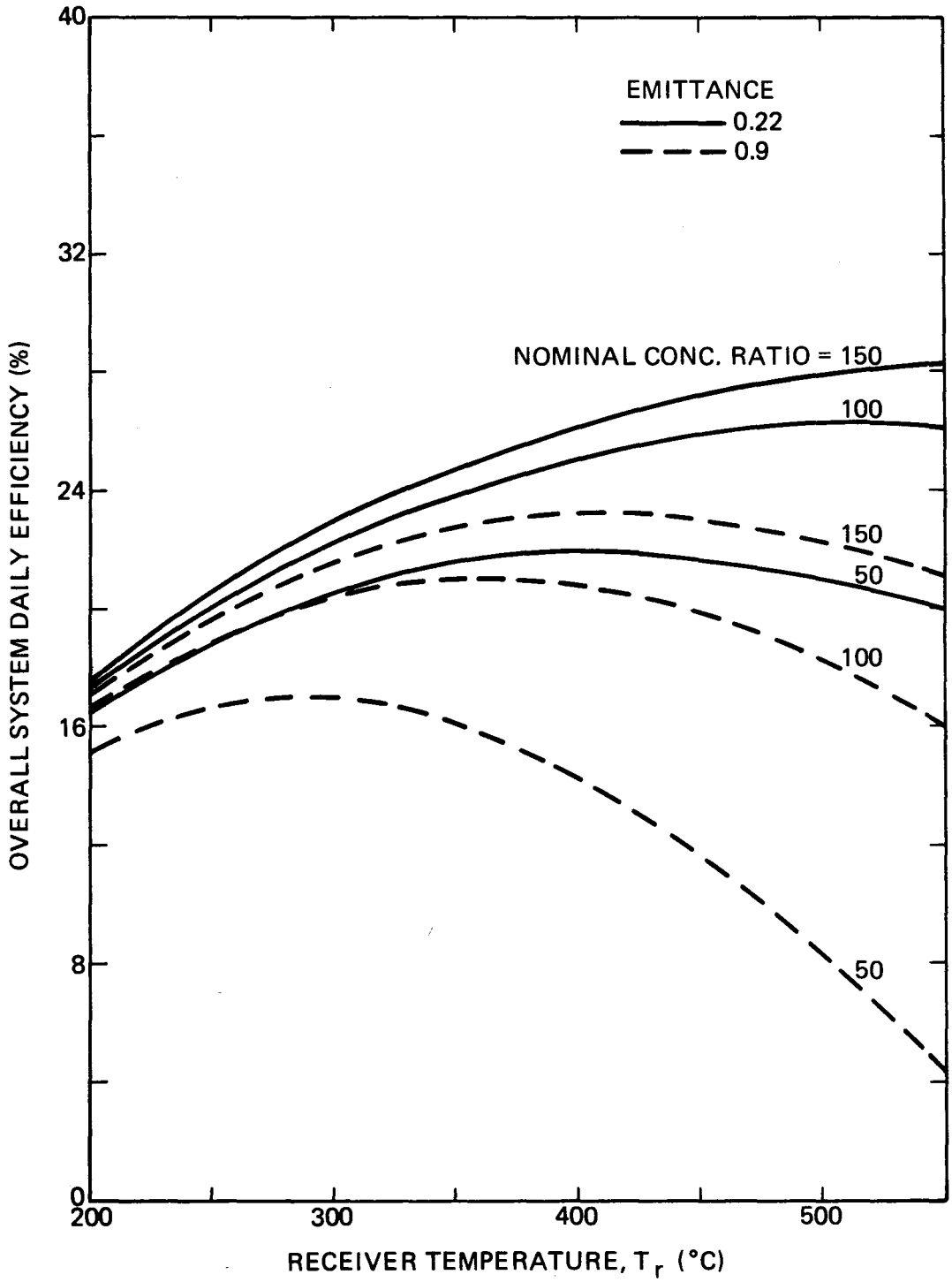

Figure 10. Influence of Concentration Ratio on System Efficiency

in the nominal concentration ratio could be a consequence of: a change in rim angle, a change in the nominal hemipsherical concentration ratio, or a combination of changes in these two quantities. A change in the nominal hemispherical concentration ratio would stem from a desire to change the intercept factor γ, or it would be a consequence of changes in the tracking or mirror accuracy. Results are given in Figure 10 for nominal concentration ratios of 50, 100, and 150 for emittances of 0.22 and 0.9. An increase in nominal concentration ratio above 100 has an appreciable influence for the high emittance absorber; however, a change from 100 to 150 results in less than a 2 percent increase in efficiency for absorber temperatures below 500°C with an absorber emittance of less than 0.22.

The influence of the optical efficiency on the overall system daily efficiency is shown in Figure 11. Results are given for optical efficiencies of 1.0 (no optical losses), 0.8, 0.6, and 0.4. The influence of the optical efficiency is indeed strong. A change in η_0 of only 0.1 results in approximately a 4 percent change in overall system daily efficiency for the range $1 \leq \eta_0 \leq 0.4$ and $300°C < T_r < 500°C$. This strong influence of η_0 means that the increase in optical losses which results from the addition of a cover plate can probably not be offset by the consequential decrease in heat loss effected by the cover plate.

The influence of the time of the year is given in Figure 12 which also shows the effect of the slope of the aperture. The trend for the case of a reflector with a horizontal aperture is approximately as expected. The highest efficiencies occur at summer solstice, and the performance at winter solstice is extremely poor. The results with a slope of 34° (ℓ = S) appear illogical. Although the average daily cosine for the same length day is higher at equinox than at winter solstice, the overall system daily efficiency is lower. This is a consequence of the poor performance in the early and late portions of the sunlit hours. The angle of incidence at sunset for a latitude and slope of 34° is 73° at winter solstice, 90° at equinox, and 105° at summer solstice. The aperture at summer solstice cannot see the sun during 16 percent of the sunlit hours. The results which are given in Appendix A show that the total energy generated throughout the day with an aperture area of 10^4 m^2 and a slope of 34° is 21.3, 21.5, and 26.7 megawatt hours at summer solstice, winter solstice, and vernal equinox, respectively.

A breakdown of the cosine, optical, heat, and Carnot losses for receiver temperatures ranging from 200 to 700°C (392 to 1292°F) is shown in Figure 13. The cosine loss differs from the average daily cosine because the influence of the zenith angle on the attenuation of the direct normal insolation by the atmosphere is included. The cosine loss is an inherent part of the SRTA collector system. The magnitude of this penalty must be carefully weighed against the advantages of the fixed reflector.

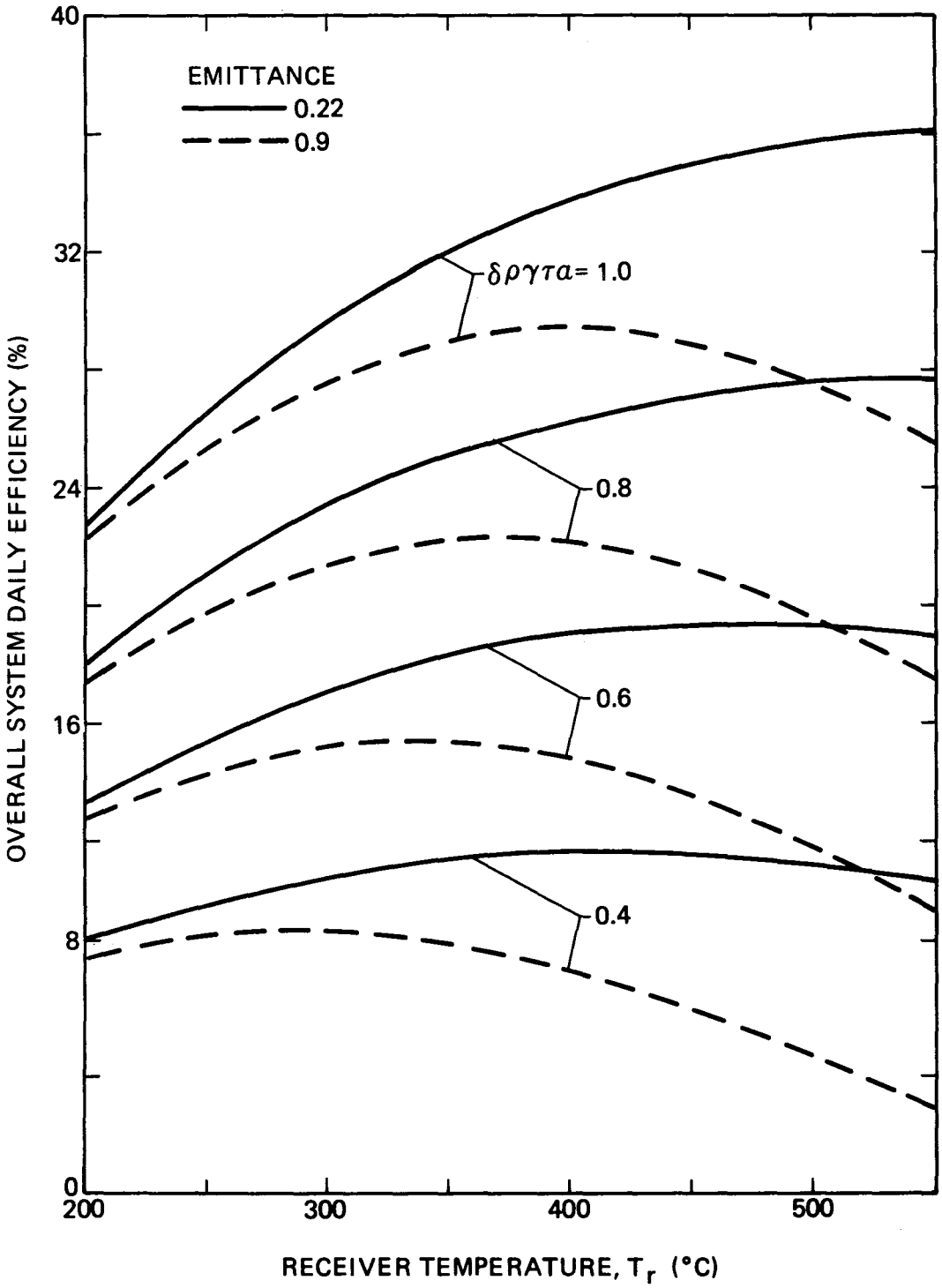

Figure 11. Influence of Optical Losses on System Efficiency

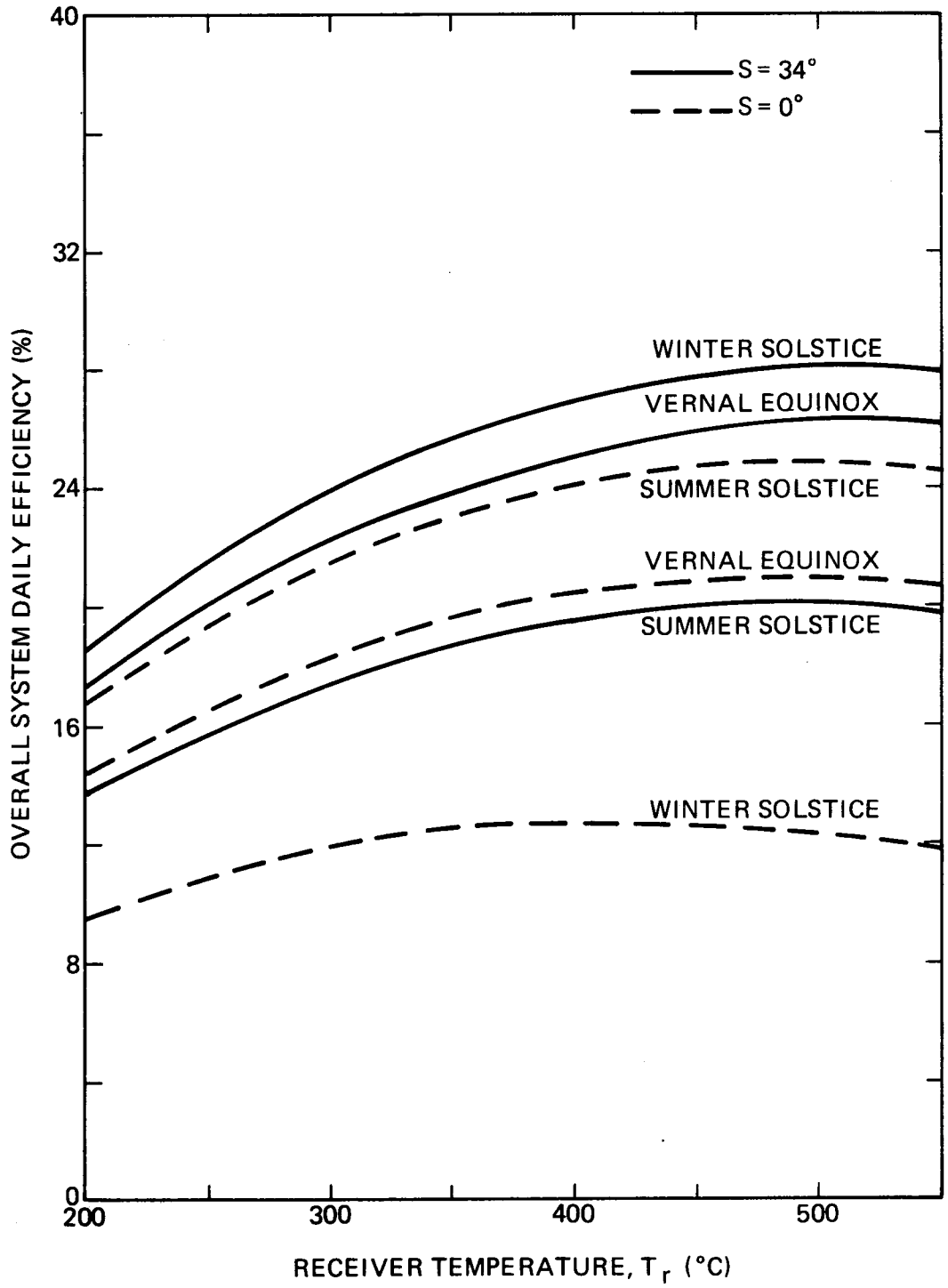

Figure 12. Influence of Time of Year and Aperture Slope on System Efficiency

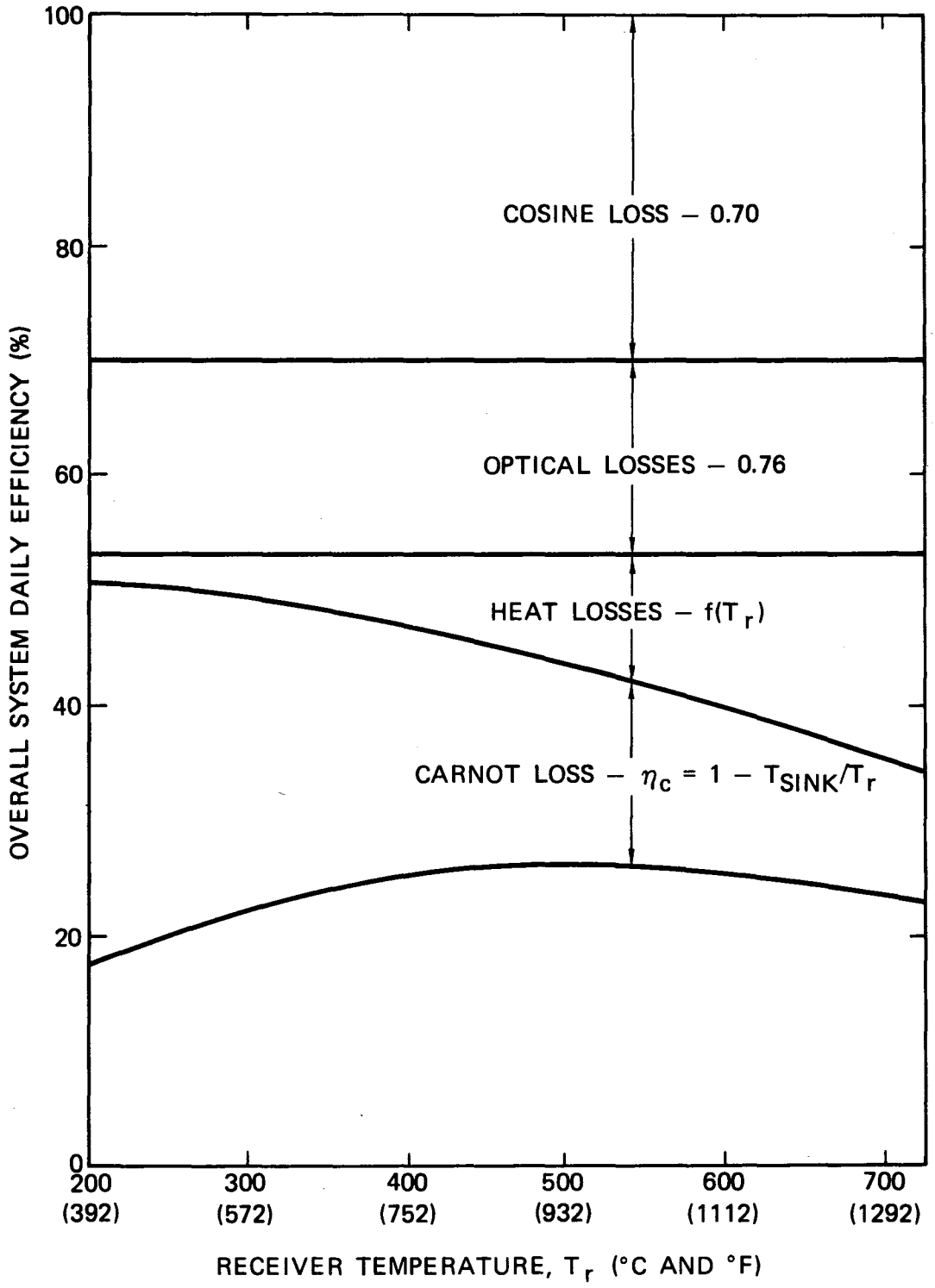

Figure 13. Comparison of Cosine, Optical, Thermal, and Carnot Losses

The optical losses are dependent on the system design and on the material properties. Since these results are based on a relatively high optical efficiency (0.76), the optical losses cannot be reduced significantly from those given in Figure 13. The second lowest curve, i.e., the one obtained by excluding the Carnot loss, gives the efficiency of the collector system if it were to supply thermal energy.

The Carnot loss shown in Figure 13 is the minimum conversion loss. Actual cycles, such as a Rankine cycle, and the addition of turbine, generator, and parasite losses will result in significantly lower efficiencies. Little can be done to reduce the conversion loss without increasing the temperature of the receiver or reducing the sink temperature.

Conclusions

It is difficult to predict the ultimate role to be played by the stationary reflector/tracking absorber solar collector. A fixed reflector should result in a reduction in cost over tracking reflectors. However, the cosine loss and the low effective concentration ratio result in relatively low efficiencies if the system is to be used for power generation. On the other hand, the complexity and cost of the two-axis tracking absorber limits the usefulness of the SRTA collector for solar heating and cooling applications in individual residences. Conclusions evident from the study are:

1. The SRTA collector provides power over a relatively short day with wide variations in power output from its sharp peak at solar noon. A tracking paraboloid, the central receiver system, and parabolic troughs result in flatter output curves. The sharply peaked output of the SRTA collector means that a large amount of storage is required for any type of intermediate or base load electrical plant. Thermal storage would result in a further degradation of the energy, which would compound the problem caused by the low effective concentration ratio.

2. The winter performance of an SRTA collector with a horizontal aperture would generally not be acceptable at latitudes within the United States. The optimum slope of the collector for year-around, clear day performance is approximately equal to the latitude. A fixed aperture collector cannot effectively utilize long summer days; consequently, the average daily cosine for a fixed length day is not a strong function of the time of the year if the collector is sloped at an angle approximately equal to the latitude. Thus the use of a day with a fixed length in the calculation of average yearly cosines is a good approximation.

The clear day output of a collector with $S = \ell$ at winter solstice is approximately equal to its output at summer solstice.

3. The cosine loss is appreciable even at the best time of the year. This loss is inherent in a collector with a fixed aperture.

4. The overall system performance is strongly dependent on the optical efficiency. The additional transmission loss associated with a cover plate, with energy incident at large angles, can probably not be offset by the reduction in heat losses which is effected by the cover plate.

5. Selective surfaces result in large improvements in performance. The increase in the overall efficiency when the ratio of the absorptance to emittance is increased from 1 to 4 is especially large.

6. The reduction in concentration ratio which results with rim angles less than 90° causes a significant degradation in collector efficiency which offsets, to a large degree, the benefit gained by the decrease in the ratio of mirror area to aperture area. The results indicate that rim angles below approximately 60° will be unsatisfactory.

7. The plane of the aperture must be tilted toward the south at typical latitudes in the continental United States in order to obtain good year-around performance. This means that an ideal site for the SRTA collector is the south slope of a steep hill or mountain. This would partially alleviate the high wind loads, large environmental impact, and high construction costs of large tilted bowls. A large array of small bowls does not appear to be a viable alternative because of the energy transport losses and the large cost of the associated plumbing.

8. The thermal design of the absorber for the SRTA collector is a difficult task because of the large axial and circumferential variations in the energy distribution which occur. The problem is further complicated by the dependence of this energy distribution on both the time of the day and the time of the year.

APPENDIX

TABULATED DIURNAL VARIATIONS

Appendix

Diurnal Variations at Vernal Equinox (Standard Case)

SYSTEM PARAMETERS:

AREA=.1000E+05	CONC. RATIO=100.	SLOPE=34.0
RIM ANGLE=90.0	TA= 20.	TS= 20.
H.T.COEFF= 8.0	TIME INCR.= .50	SINK TEMP.=40.
EMITTANCE= .22	OPTICAL EFF.= .765	

SOLAR PARAMETERS:

DAY 81.	SUNRISE/SUNSET 6.016	STANDARD TIME 12.871
LATITUDE 33.65	LONGITUDE 101.23	DECLINATION 0.37
CLEAR. NO. 1.0	C1 .20	

CALCULATED SYSTEM PARAMETERS:

QINCD(MW-HR)= 102.	SPHERE RAD.= 56.	APER. RAD.= 56.
NET CONC. RATIO=100.0	MIRROR AREA=.200E+05	LIP HEIGHT= 63.

TIME HRS	AL	AZ	INCIDENCE	HEAT FLUX(W/SQ.M) NORMAL	APERTURE	RECEIVER
	--(DEGREES)--					
0.00	57.	180.	1.	979.	978.	66519.
0.50	56.	167.	8.	977.	968.	65781.
1.00	54.	154.	15.	973.	940.	63586.
1.50	51.	143.	23.	966.	893.	59978.
2.00	46.	134.	30.	956.	828.	55035.
2.50	42.	126.	38.	942.	747.	48867.
3.00	36.	119.	45.	923.	653.	41617.
3.50	31.	113.	53.	897.	546.	33468.
4.00	25.	107.	60.	862.	431.	24653.
4.50	19.	103.	68.	812.	311.	15474.
5.00	13.	98.	75.	741.	192.	6362.
5.50	6.	94.	83.	632.	82.	-2000.
6.00	0.	90.	90.	0.	0.	0.

TR= 500. CARNOT EFF.= 59.5%

TIME HRS	POWER MW(E)	ENERGY MW(E)-HR	EFFICIENCY (%) TOT.	APER.	NOR.	POWER/MIRROR AREA W(E)/SQ.M
0.00	3.96	0.00	0.0	40.5	40.5	198.
0.50	3.91	3.94	3.9	40.4	40.1	196.
1.00	3.78	7.78	7.6	40.3	38.9	189.
1.50	3.57	11.46	11.3	40.0	36.9	178.
2.00	3.27	14.88	14.6	39.5	34.2	164.
2.50	2.91	17.97	17.7	38.9	30.9	145.
3.00	2.48	20.66	20.3	37.9	26.8	124.
3.50	1.99	22.90	22.5	36.5	22.2	100.
4.00	1.47	24.63	24.2	34.0	17.0	73.
4.50	0.92	25.82	25.4	29.6	11.3	46.
5.00	0.33	26.47	26.0	19.7	5.1	19.
5.50	0.00	26.66	26.2	0.0	0.0	0.

Diurnal Variations at Summer Solstice

SYSTEM PARAMETERS:

AREA=.1000E+05	CONC. RATIO=100.	SLOPE=34.0
RIM ANGLE=90.0	TA= 20.	TS= 20.
H.T.COEFF= 8.0	TIME INCR.= .50	SINK TEMP.=40.
EMITTANCE= .22	OPTICAL EFF.= .765	

SOLAR PARAMETERS:

DAY 173.	SUNRISE/SUNSET 7.123	STANDARD TIME 12.772
LATITUDE 33.65	LONGITUDE 101.23	DECLINATION 23.52
CLEAR. NO. 1.0	C1 .20	

CALCULATED SYSTEM PARAMETERS:

QINCD(MW-HR)= 106.	SPHERE RAD.= 56.	APER. RAD.= 56.
NET CONC. RATIO=100.0	MIRROR AREA=.200E+05	LIF HEIGHT= 63.

TIME	AL	AZ	INCIDENCE	HEAT FLUX(W/SQ.M)		
HRS	--(DEGREES)--			NORMAL	APERTURE	RECEIVER
0.00	80.	180.	24.	831.	806.	53353.
0.50	73.	145.	25.	830.	798.	52754.
1.00	73.	124.	28.	877.	775.	50969.
1.50	62.	111.	32.	872.	736.	48038.
2.00	62.	103.	38.	864.	684.	44029.
2.50	56.	97.	44.	854.	619.	39036.
3.00	50.	92.	50.	840.	542.	33133.
3.50	43.	88.	56.	822.	457.	26621.
4.00	37.	84.	63.	799.	364.	19539.
4.50	31.	81.	70.	768.	268.	12165.
5.00	25.	77.	76.	723.	171.	4792.
5.50	19.	74.	83.	676.	79.	-2245.
6.00	13.	70.	90.	604.	-1.	0.
6.50	7.	66.	97.	503.	-61.	0.
7.00	1.	62.	104.	0.	0.	0.

TR= 500. CARNOT EFF.= 59.5%

TIME	POWER	ENERGY	EFFICIENCY (%)			POWER/MIRROR AREA
HRS	MW(E)	MW(E)-HR	TOT.	APER.	NOR.	W(E)/SQ.M
0.00	3.17	0.00	0.0	39.4	36.0	159.
0.50	3.14	3.16	3.0	39.3	35.7	157.
1.00	3.03	6.24	5.9	39.1	34.6	152.
1.50	2.86	9.19	8.7	38.8	32.8	143.
2.00	2.62	11.93	11.3	38.3	30.3	131.
2.50	2.32	14.40	13.6	37.5	27.2	116.
3.00	1.97	16.55	15.6	36.4	23.5	99.
3.50	1.58	18.32	17.3	34.7	19.3	79.
4.00	1.16	19.70	18.6	31.9	14.6	58.
4.50	0.72	20.64	19.5	27.1	9.4	36.
5.00	0.23	21.15	20.0	16.6	3.9	14.
5.50	0.00	21.29	20.1	0.0	0.0	0.

Diurnal Variations at Winter Solstice

SYSTEM PARAMETERS:

AREA=.1000E+05	CONC. RATIO=100.	SLOPE=34.0
RIM ANGLE=90.0	TA= 20.	TS= 20.
H.T.COEFF= 8.0	TIME INCR.= .50	SINK TEMP.=40.
EMITTANCE= .22	OPTICAL EFF.= .765	

SOLAR PARAMETERS:

DAY 356.	SUNRISE/SUNSET 4.887	STANDARD TIME 12.714
LATITUDE 33.65	LONGITUDE 101.23	DECLINATION -23.35
CLEAR. NO. 1.0	C1 .20	

CALCULATED SYSTEM PARAMETERS:

QINCD(MW-HR)= 77.	SPHERE RAD.= 56.	APER. RAD.= 56.
NET CONC. RATIO=100.0	MIRROR AREA=.200E+05	LIP HEIGHT= 63.

TIME HRS	AL	AZ	INCIDENCE	HEAT FLUX(W/SQ.M) NORMAL	APERTURE	RECEIVER
	--(DEGREES)--					
0.00	33.	190.	23.	945.	870.	58222.
0.50	33.	172.	24.	943.	860.	57500.
1.00	31.	164.	27.	936.	832.	55348.
1.50	29.	156.	32.	924.	786.	51809.
2.00	26.	149.	37.	906.	722.	46953.
2.50	23.	143.	43.	880.	643.	40881.
3.00	19.	137.	49.	843.	549.	33728.
3.50	14.	131.	56.	791.	444.	25667.
4.00	9.	126.	63.	715.	330.	16933.
4.50	4.	122.	69.	598.	212.	7880.

TR= 500. CARNOT EFF.= 59.5%

TIME HRS	POWER MW(E)	ENERGY MW(E)-HR	EFFICIENCY (%) TOT.	APER.	NOR.	POWER/MIRROR AREA W(E)/SQ.M
0.00	3.46	0.00	0.0	39.8	36.7	173.
0.50	3.42	3.44	4.5	39.8	36.3	171.
1.00	3.29	6.80	8.8	39.6	35.2	165.
1.50	3.08	9.99	13.0	39.2	33.4	154.
2.00	2.79	12.93	16.8	38.7	30.8	140.
2.50	2.43	15.54	20.2	37.8	27.6	122.
3.00	2.01	17.76	23.1	36.5	23.8	100.
3.50	1.53	19.52	25.4	34.4	19.3	76.
4.00	1.01	20.79	27.1	30.5	14.1	50.
4.50	0.47	21.53	28.0	22.2	7.8	23.

REFERENCES

1. W. G. Steward, "A Concentrating Solar Energy System Employing a Stationary Spherical Mirror and Movable Collector," Proceedings of NSF/RANN Workshop on Solar Heating and Cooling for Buildings, Washington, D. C., 1973, pp. 24-25.

2. W. G. Steward and F. Kreith, "Stationary Concentrating Reflector cum Tracking Absorber Solar Energy Collector: Optical Design Characteristics," Applied Optics, Vol. 14, No. 7, July 1975, pp. 1509-1512.

3. J. F. Kreider, "Thermal Performance Analysis of the Stationary Reflector/Tracking Absorber (SRTA) Solar Concentrator," ASME J. of Heat Transfer, Vol. 97, Series C, No. 3, August 1975, pp. 451-456.

4. The American Ephemeris and Nautical Almanac for the Year 1977, Nautical Almanac Office, U. S. Naval Observatory, U. S. Government Printing Office, Washington, D. C., 1975.

5. American Society of Heating, Refrigerating, and Air Conditioning, "Procedure for Determining Heating and Cooling Loads for Computerized Energy Calculations," 1971, pp. 18-24.

6. J. L. Threlkeld, Thermal Environmental Engineering, Prentice-Hall, 1972, p. 299.

7. R. B. Pettit, Correspondence of May 26, 1976, Sandia Laboratories, Albuquerque, New Mexico.

UNLIMITED RELEASE

INITIAL DISTRIBUTION:

U.S. ERDA (4)
Washington, D.C. 20545
Attn: R. Blieden
H. Marvin
G. Kaplan
L. Melamed

U.S. ERDA
Albuquerque Operations Office
P. O. Box 5400
Albuquerque, NM 87115
Attn: D. K. Nowlin

U.S. ERDA
Sandia Area Office
P. O. Box 5400
Albuquerque, NM 87115
Attn: R. Duval

Sheldahl, Inc. (2)
Northfield, MN 55057
Attn: Dr. D. E. Anderson
R. A. Stickley

Los Alamos Scientific Laboratory
Los Alamos, NM 87544
Attn: Dr. Douglas Balcomb

Electric Power Research Institute (3)
3412 Hillview Avenue
Palo Alto, CA 94304
Attn: J. Cummings
P. Bos
J. Bigger

Southern California Edison
2244 Walnut Grove Avenue
Rosemead, CA 91770
Attn: G. W. Braun

Lawrence Livermore Laboratory
P. O. Box 808
Livermore, CA 94550
Attn: Dr. William Dickinson, L-14

General Atomic Company
P. O. Box 81608
San Diego, CA 92138
Attn: G. H. Eggers

L. L. Vant Hull
University of Houston
Department of Physics
3801 Cullen Boulevard
Houston, TX 77004

Argonne National Laboratory
Argonne, IL 60439
Attn: John Martin

Prof. Aden B. Meinel
Optical Sciences Center
University of Arizona
Tucson, AZ 85721

Mervin Brown
Arizona Public Service Company
P. O. Box 21666
Phoenix, AZ 85036

Dean B. McKenney
Helio Associates, Inc.
P. O. Box 17960
Tucson, AZ 85731

Y. P. GUPTA
E-Systems, Inc.
P. O. Box 6118
Dallas, TX 75222
Attn: R. R. Walters

John D. Reichert
Department of Electrical Engineering
Texas Tech University
Lubbock, TX 79409

M. Watson
Aerospace Corporation
Energy and Transportation Division
2350 East El Segundo Blvd.
El Segundo, CA 90245

W. G. Steward
Sugarloaf Road
Boulder, CO 80302

Frank Kreith
University of Colorado
Boulder, CO 80302

J. F. Kreider
Environmental Consulting Services, Inc.
Boulder, CO 80302

J. Plamondon
Jet Propulsion Laboratory
4800 Oak Grove Drive
Pasadena, CA 91103

U.S. ERDA
Division of Headquarters Services
Library Branch, Room G-049
Washington, D.C. 20545

T. B. Lane, 1540
H. C. Hardee, 1543
A. Narath, 5000
J. H. Scott, 5700
G. E. Brandvold, 5710
R. P. Stromberg, 5711
J. A. Leonard, 5712
M. Edenburn, 5719
R. C. Heckman, 5842
T. B. Cook, Jr., 8000
L. Gutierrez, 8100
A. N. Blackwell, 8110
A. F. Baker, 8111
C. S. Selvage, 8180
A. C. Skinrood, 8184 (3)
T. D. Brumleve, 8184 (5)
A. M. Clausing, 8184 (8)
C. H. DeSelm, 8200
B. F. Murphey, 8300
T. S. Gold, 8320
R. L. Rinne, 8321
R. Lee, 8322
W. C. Scrivner, 8400
Technical Publications and Art Division, 8265, for TIC (2)
F. J. Cupps, 8265/Technical Library Processes Division, 3141
Technical Library Processes Division, 3141 (4)
Library and Security Classification Division, 8266 (5)